

# **inter·noise 2002**

**The 2002 International Congress and Exposition on Noise Control Engineering**  
*Dearborn, MI, USA. August 19-21, 2002*

## **TRANSIENT RESPONSE OF A HYDRAULIC ENGINE MOUNT**

R. Singh, H. Adiguna and M. Tiwari  
Acoustics and Dynamics Laboratory, Center for Automotive Research  
The Ohio State University, Columbus, OH 43210-1107 USA

H. Tseng and D. Hrovat  
Scientific Research Laboratory, Ford Motor Company  
Dearborn, MI 48124, USA

### **Abstract**

Transient response of a typical hydraulic engine mount is studied using analytical and experimental methods. First, a lumped parameter nonlinear model is used to formulate the problem and to suggest parameters that must be experimentally determined. Several configurations as related to inertia track and decoupler are analyzed. Second, two bench experiments are constructed for the identification of nonlinear chamber compliances (with and without pre-loads) and nonlinear fluid resistances. Third, the nonlinear characteristics of decoupler are described to accurately predict the time events of the decoupler gap opening and closing. An equivalent viscous damper model is employed along with a multi-staged switching mechanism. Forth, nonlinear behavior arising due to the vacuum formation in the top chamber is studied by defining a bi-linear asymmetric stiffness curve. All governing equations are then solved in time domain to yield responses when step up, step down or triangular displacement waveforms are applied. New transient experiments are also conducted on an elastomer test system by applying known displacement inputs, and measured transmitted force and top chamber pressure signals are analyzed in time and frequency domains. Results of the proposed simulation model match well with measured data.

### **1. Introduction**

Hydraulic engine mounts are designed and tuned to provide amplitude-sensitive and spectrally varying properties [1-5]. The performance is typically measured on a steady state basis using the sinusoidal non-resonant type test method [2-4] that is then employed for product design and quality control. Nevertheless, their transient characteristics are poorly understood, and the relevant simulation methods and experimental techniques are not readily available. Therefore, the chief objective of this article is to summarize

simulation models that may be utilized to design, specify and diagnose the transient characteristics arising due to many vehicle conditions such as travel on bumpy roads, abrupt accelerations or decelerations, garage shift events, braking, and cornering.

## 2. Non-Linear Simulation Model

The concept of the hydraulic mount is illustrated in Figure 1 where  $u(x,t)$  is the hydraulic reaction force. Here  $q_i$ ,  $q_d$ ,  $p_1$ ,  $p_2$ ,  $\bar{p}$ ,  $x$ ,  $A_p$ , and  $F_T$  denote the flow rate through inertia track (# i), flow rate through decoupler (# d), top chamber (# 1) pressure, bottom chamber (# 2) pressure, pressure at static equilibrium condition, displacement excitation, equivalent piston area, and transmitted force, respectively.

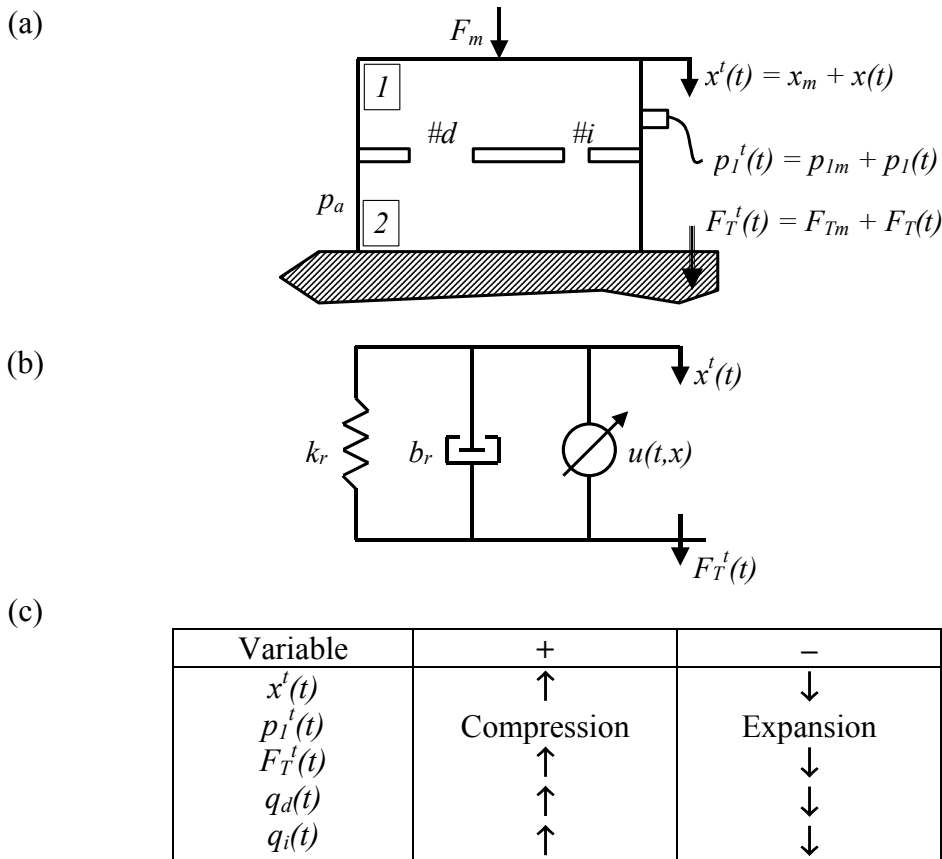


Figure 1. Hydraulic mount concept. (a) Measured variables, (b) Force transmission paths, and (c) Sign convention where  $\uparrow$  implies an upward motion and  $\downarrow$  refers to the downward motion.

The mount is modeled by lumping the fluid system into several control volumes as shown in Figure 2. The system parameters include the top and bottom chamber fluid compliances ( $C_1$  and  $C_2$ ), elastomeric element stiffness ( $k_r$ ) and damping ( $b_r$ ), inertia

track inertance ( $I_i$ ) and fluid resistance ( $R_i$ ), and decoupler resistance ( $R_d$ ). Through experimentation, it is shown that  $C_1$ ,  $C_2$ ,  $R_i$ , and  $R_d$  have nonlinear characteristics [2, 4]. The momentum and continuity equations yield the following equations; refer to [1-5] for details.

$$q_i(t) + q_d(t) = A_p \dot{x}(t) - C_1(p_1) \dot{p}_1(t) \quad (1)$$

$$-q_i(t) - q_d(t) = C_2(p_2) \dot{p}_2(t) \quad (2)$$

$$F_T(t) = b_r \dot{x}(t) + k_r x(t) + A_p(\bar{p} - p_1(t)) \quad (3)$$

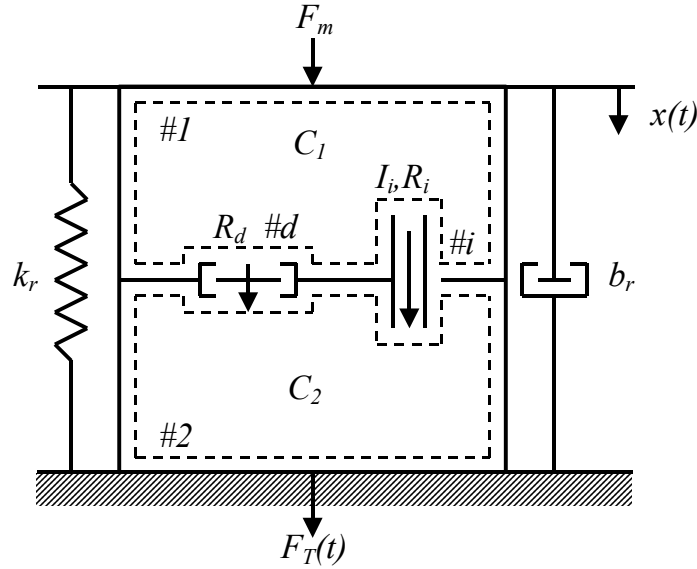


Figure 2. Lumped parameter model.

The inertia track is modeled by the following differential equation where the  $R_i$  term depends on fluid variables.

$$I_i \dot{q}_i(t) + R_i(\Delta p_{12}, q_i) q_i(t) = p_2(t) - p_1(t) = \Delta p_{12}(t) \quad (4)$$

In general, the relation between steady state pressure drop ( $\Delta p_{12}$ ) and steady flow rate ( $q_i$ ) in a pipe is nonlinear:  $q_i = C_d A_i \sqrt{2\Delta p_{12}/\rho}$  where  $C_d$  is the coefficient of discharge. In our work,  $R_i$  is determined via a bench experiment [2, 4]. For the case of a free-floating decoupler, the fluid flow is controlled by the decoupler switching mechanism, which couples or decouples the inertia track. On the other hand, when the disk is at the top or at the bottom,  $q_d$  is zero, and thus the fluid can only flow through the inertia track. A linear model of the decoupler is given by a first order differential equation (5) where  $b_v$  and  $A_d$  denote the viscous damping coefficient and cross-sectional area of the decoupler gap. Further,  $m_d$  and  $x_d$  represent the disk mass and displacement of the decoupler.

$$m_d \ddot{x}_d(t) + b_v \dot{x}_d(t) = A_d [p_2(t) - p_1(t)]; \quad \dot{x}_d(t) = \frac{q_d(t)}{A_d} \quad (5a-b)$$

Experimentally, the dynamics of decoupler is studied by installing a pressure transducer in the top chamber. The closing and opening events of the decoupler can be clearly observed in the top chamber pressure  $p_1(t)$ .

A nonlinear simulation model in the Matlab/Simulink environment is developed. Except for the decoupler, nonlinear components can be modeled via continuous nonlinear functions. Such continuous relationships are obtained either experimentally or via mathematical descriptions of the physical processes. Some nonlinearities can be linearized provided the dynamic excursion range is small. This holds true for  $p_2(t)$  because  $C_2$  is very high and the associated dynamic excursions are close to the atmospheric pressure. In addition, the top pressure chamber exhibits an asymmetric nonlinearity because of the vacuum formation. Nevertheless, the stiffness in both regimes is treated as linear with very different slopes and the transition at  $p_1 = p_a$  is assumed continuous. In some cases, the polynomial curve-fit is employed. The nonlinear model is solved employing the 4<sup>th</sup> order Runge-Kutta method with a fixed time step. The total time to run the steady state simulation model for a particular  $X$  and  $f$  of excitation is specified by  $60T$  where  $T = 1/f$  is the period of excitation. Of the  $60T$  time span, the first  $40T$  is used to overcome the starting transient effects. Data from the rest of the time ( $20T$ ) is used for time or frequency domain validation process. The free decoupler model consumes more time due to the additional nonlinearity introduced by the decoupler mechanism.

A comparison of experimental results between the fixed ( $R_d \rightarrow \infty$ ) and free decoupler (finite  $R_d$ ) cases shows that the nonlinearity is caused mostly by the vacuum pressure created in the top chamber and the decoupler switching action. The elimination of decoupler focuses the study on the formation of vacuum, which is still poorly understood. The initial conditions for  $p_1(t)$  and  $p_2(t)$  are set as atmospheric pressure  $p_a$ . Since the compliance of each chamber is nonlinear, at each time step, the operating pressure is used to estimate  $C_1$  and  $C_2$  from the measured  $p$ - $V$  curves. Each compliance ( $C_1$  or  $C_2$ ) is expressed as a polynomial function of pressure ( $p_1$  or  $p_2$ ). The dynamic pressures  $p_1(t)$  and  $p_2(t)$  calculated throughout the simulation are gage pressures (above or below  $p_a$ ). The inertia track sub-system is constructed based on equation (4). The  $\Delta p_{12}$  due to  $R_i$  element is utilized as a feedback loop to this system. The nonlinear resistance  $R_i$  is specified as a function of  $q_i$ . The initial condition for  $q_i$  is zero since the simulation is assumed to start from the static equilibrium condition. The transmitted force sub-system calculates the components contributed by both rubber and fluid elements, as shown by equation (3). The rubber stiffness  $k_r$  and damping  $b_r$  are interpolated from measured data by employing a look-up table, while  $p_1$  is calculated numerically from the top chamber sub-system.

In the free decoupler model, yet another sub-system associated with a free-floating disk is integrated in the mount model. The equation for motion for the decoupler gap is based on (5) derived for the dashpot model. The decoupler sub-system has to be enabled or disabled depending whether the decoupler opens or closes. The states of the system such as  $\dot{x}_d$  and  $x_d$  have to be held or reset to zero whenever the decoupler closes. To better

understand the phenomenon, the sequence of events is divided into 5 stages. Stage 1: Initially, the disk is assumed to be at the top ( $x_d = \Delta_d$ ) and the gap is closed, and hence  $q_d = 0$  and  $q = q_i$ . Stage 2: When  $p_1 > p_2$ , the decoupler starts to move down (open) and as a result, the fluid flow through the decoupler  $q_d$  tries to equalize the  $p_1$  and  $p_2$ , and oppose an increase in  $p_1$ . Notice that  $q_i$  is still  $> 0$  although the disk is moving downward. This is due to the inertance effect of the inertia track. Stage 3: The disk is at the bottom ( $x_d = 0$ ) and the decoupler gap is closed ( $q_d = 0$ ). Due to the decreasing  $q_i$ ,  $p_1$  increases. Then  $q_i$  changes direction, which causes  $p_1$  to decrease. Stage 4: When  $p_1 < p_2$ , the disk starts to move up (gap is now open), and the  $p_1$  suddenly stops varying until the decoupler is closed again. Stage 5: The decoupler disk is at the top, and as  $x(t)$  and  $q_i$  move upward. Vacuum is now generated. During this stage,  $p_1 < p_2$  and  $p_1 < p_a$ . When  $x(t)$  changes direction,  $p_1$  again starts to increase. Stages 2 to 5 continue to repeat themselves.

### 3. Experimental Methodology

Bench experiments are constructed to study the nonlinear characteristics of  $C_1$ ,  $C_2$ , and  $R_i$ . The objectives of these experiments are to determine whether the nonlinear characteristics can be modeled by simplified theoretical expressions. Alternatively, empirical results must be incorporated in simulation. Sinusoidal or transient dynamic tests have been done using the MTS (model 831.50, 1000 Hz) elastomer test system [4]. Two configurations of the take-apart mount are used for study: (a) free decoupler mount (with both decoupler and inertia track) and (b) fixed decoupler mount (without any decoupler). The take-apart mount is assembled in a water bath so as not to include any air. The assembly is done with a clamping fixture. Care has to be taken that there are no bubbles in the water bath, which can be trapped during the assembly of the mount. For maintaining a low level of dissolved air, the water temperature should be kept low. The internal dynamics is studied by installing a pressure transducer in the top chamber and measuring the dynamic  $p_1(t)$ . This can accurately map the dynamic stages of the decoupler as  $p_1(t)$  waveform gives a very good understanding of the internal dynamics. Two kinds of pressure transducer were used for experimentation: (a) absolute pressure transducer (strain gage), and (b) dynamic pressure transducer (piezoelectric). The absolute pressure transducer is primarily used for recording the mean  $\bar{p}_1$  level, while the dynamic pressure transducer is used for accurately recording  $p_1(t)$ . Under the static manual control of the MTS controller, the mount was subjected to varying loads and  $\bar{p}_1$  was recorded. This gave an estimate of the initial pressure to be used for simulation.

A transient displacement input  $x(t)$  was applied to the mount using the MTS system. The servo hydraulic system was programmed in the displacement control mode for applying a single ‘rectangular’ (step up and step down), triangular and sawtooth waveforms. All such excitations were applied over a mean displacement input  $x_m$  corresponding to  $F_m = -1200$  N. The top chamber pressure  $p_1(t)$ , transmitted force  $F_t(t)$ , and displacement excitation  $x(t)$  signals were acquired and processed using the digital system that is independent of the MTS machine.

## 4. Transient Response

Transient response simulations are conducted by applying step and pulse displacement inputs corresponding to the experimental waveforms. For example, Figure 3 shows the measured waveforms corresponding to step up and down transients. The step up displacement of Figure 3 is obtained by applying a 1200 N (say  $B$ ) compressive preload, and then releasing it to 0 N (say  $A$ ); the procedure is reversed for step down. The  $F_T(t)$  peak during the step up ( $B$  to  $A$ ) is less than the force transmitted during the step down ( $A$  to  $B$ ) as shown in Figure 3. This further strengthens our claim that the mount behaves in an asymmetric manner. The role of vacuum formation is very dominant in controlling such an asymmetric behavior.

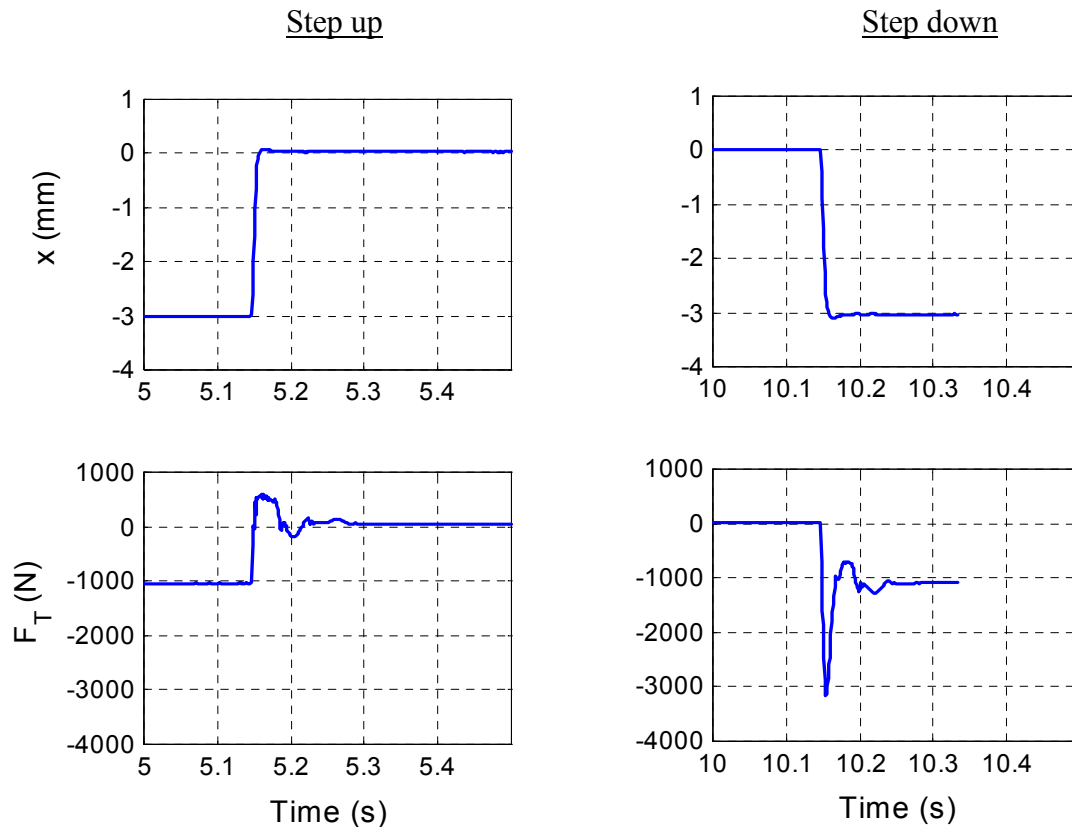


Figure 3. Measured step up and step down displacement excitation and transmitted force waveforms for a free decoupler mount.

The pulse input of Figures 4 and 6 is acquired by applying a preload  $B = 1200$  N, releasing to  $A = 0$  N in 0.1 s and compressing it again to  $B$  in yet another 0.1 s. There is a limit to the pulse width that can be achieved by a servo-hydraulic test system, when subjecting the mount to a gradual ramp. A further reduction in the pulse time makes it difficult to achieve the peak amplitude. The transmitted force  $F_T(t)$  and top chamber pressure  $p_l(t)$  from simulation and experiment match very well for both fixed and free decouplers in Figures 4 and 5. Note that the  $p_l$  is measured using a dynamic transducer with a lower frequency limit of 0.5 Hz. Consequently, measured results show a very low

frequency trend or drift. Such trends are not obviously seen in simulations. For the free decoupler case,  $q_i$ ,  $q_d$ , and  $x_d$  time histories are plotted for a better understanding of the inertia track dynamics and the decoupler switching mechanism. Figure 5 shows that when compared to the case of fixed decoupler (Figure 4), the addition of a free decoupler results in reduced oscillations. This suggests that the decoupler introduces damping to the system. Decoupler action comes out very prominently in the simulated waveforms (Figure 5) of  $p_l$  and  $F_T$ . As the decoupler closes,  $p_l$  rises significantly as shown by the small ‘bumps’. The disk displacement  $x_d$  is also plotted to illustrate the sequencing mechanism. One final note regarding the measured  $p_l(t)$  histories is that  $p_l$  is measured using a dynamic transducer with a lower frequency limit of 0.5 Hz. Consequently, measured results show a very low frequency trend or drift. Such trends are not obviously seen in simulations. More transient results can be found in [5].

## 5. Conclusion

The dynamic response of a typical hydraulic engine mount to transient excitations has been theoretically and experimentally analyzed. This work is new and in the process, we had to investigate the steady state behavior as well. New dynamic experiments have also been conducted given step, pulse (triangle) and sawtooth displacement profiles. A new switching model of the decoupler based on an equivalent viscous damping mechanism concept is used and this formulation matches well with transient measurements. The proposed simulation model can be integrated within a larger vehicle dynamic model. Finally, the experimental procedure we have used could lead to a standard transient test and correlation method with real-life events.

## Acknowledgement

We gratefully acknowledge the research support from the Ford Motor Company. Experimental studies were made possible by equipment grants from the Ohio Board of Regents and the MTS Systems Corporation. Finally, we acknowledge Delphi Automotive (Chassis) for supplying the mounts.

## References

1. R. SINGH, G. KIM and P. V. RAVINDRA 1992 *Journal of Sound and Vibration* **158(2)**, 219-243. Linear analysis of automotive hydro-mechanical mount with emphasis on decoupler characteristics.
2. G. KIM and R. SINGH 1993 *ASME Journal of Dynamic Systems, Measurement and Control* **115**, 482-487. Nonlinear analysis of automotive hydraulic engine mount.
3. G. KIM and R. SINGH 1995 *Journal of Sound and Vibration* **179(3)**, 427-453. Study of passive and adaptive hydraulic engine mount systems with emphasis on nonlinear characteristics.
4. M. TIWARI, H. ADIGUNA and R. SINGH 2002 submitted to the *Noise Control Engineering Journal*. Experimental characterization of a nonlinear hydraulic engine mount.
5. H. ADIGUNA, M. TIWARI, R. SINGH, H.E.TSENG AND D.HROVAT 2002 submitted to the *Journal of Sound and Vibration*. Transient response of a hydraulic engine mount.

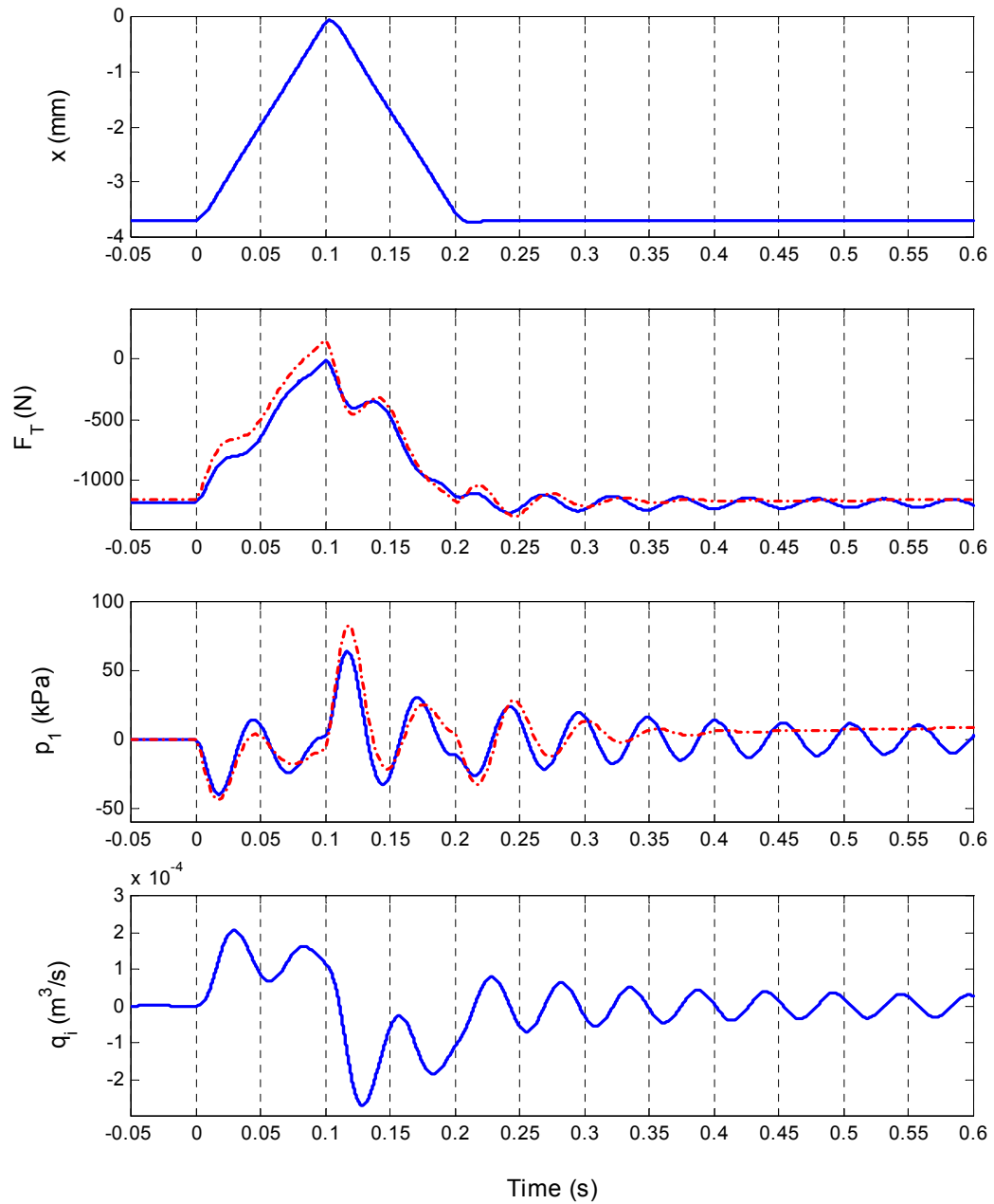


Figure 4. Pulse response of the fixed decoupler mount.  
 Key for  $F_T$  and  $p_1$  plots: — (blue) Simulation, --- (red) Measured.



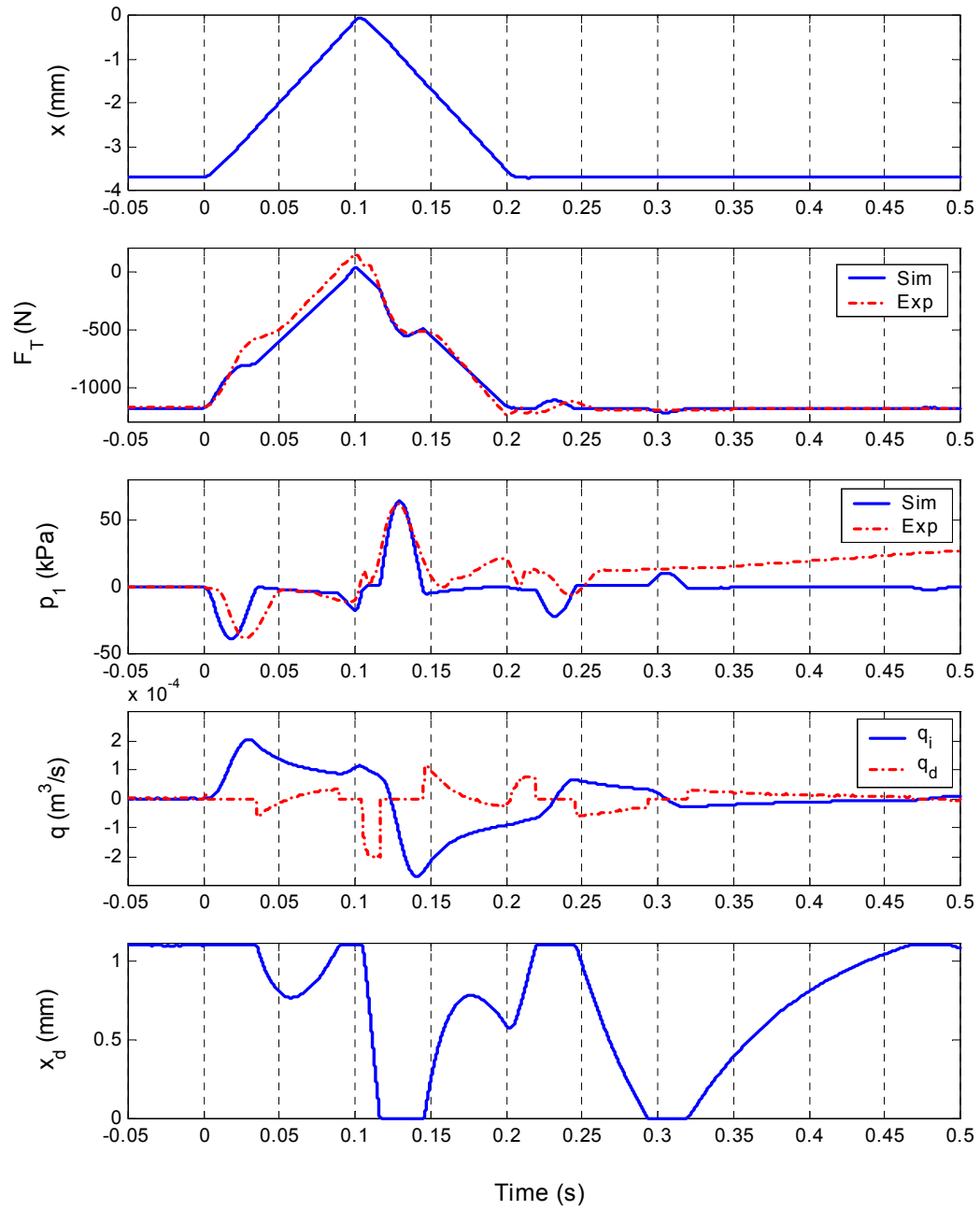


Figure 5. Pulse response of the free decoupler mount.  
 Key for  $F_T$  and  $p_1$  plots: — (blue) Simulation, - - - (red) Measured.